Ward De Paepe[1]
Faculty of Engineering,
University of Mons (UMONS),
Thermal Engineering and Combustion Unit,
Place du Parc 20,
Mons 7000, Belgium
e-mail: ward.depaepe@umons.ac.be

Alessio Pappa
Faculty of Engineering,
University of Mons (UMONS),
Thermal Engineering and Combustion Unit,
Place du Parc 20,
Mons 7000, Belgium
e-mail: alessio.pappa@umons.ac.be

Diederik Coppitters
Faculty of Engineering,
University of Mons (UMONS),
Thermal Engineering and Combustion Unit,
Place du Parc 20,
Mons 7000, Belgium email:
Diederik.coppitters@umons.ac.be

Marina Montero Carrero
Faculty of Engineering,
Vrije Universiteit Brussel (VUB), Thermo and
Fluid Dynamics (FLOW),
Brussel 1050, Belgium,
e-mail: mmontero@vub.ac.be

Panagiotis Tsirikoglou
Limmat Scientific AG,
Industriestrasse 7,
Zug CH-6300, Switzerland
e-mail: tsirikoglou@limmatscientific.ch

Francesco Contino
Faculty of Engineering,
Université catholique de Louvain (UCLouvain)
Thermodynamics and Fluid Mechanics,
Place du Levant, 2,
Louvain-la-Neuve 1348, Belgium
e-mail: francesco.contino@uclouvain.ac.be

Recuperator Performance Assessment in Humidified Micro Gas Turbine Applications Using Experimental Data Extended With Preliminary Support Vector Regression Model Analysis

Cycle humidification applied to micro gas turbines (mGTs) offers a solution to overcome their limited operational flexibility in terms of variable electrical and thermal power production when used in a combined heat and power (CHP) application. Although the positive impact of this cycle humidification on the performance has already been proven numerically and experimentally, very detailed modeling of the system performance remains challenging, especially the determination of the recuperator effectiveness, which has the highest impact on the final cycle performance. Indeed, the recuperator performance depends strongly on the mass flow rate of the air stream and its humidification level, two parameters that are difficult to measure accurately. Accurate modeling of the recuperator performance under both dry and humidified conditions is thus essential for correct assessment of the potential of humidified mGT cycles in decentralized energy systems (DESs). In this paper, we present a detailed analysis of the recuperator performance under humidified conditions using averaged experimental data, extended with the application of a support vector regression (SVR) on a time series to improve noise-modeling of the output signal, and thus enhance the accuracy of the monitoring process. In a first step, the missing experimental parameters, air mass flow rate and humidity level, were obtained indirectly, using rotational speed, fuel flow rate, exhaust gas composition and pressure level measurements in combination with the compressor map. Despite the low accuracy, some general trends regarding the recuperator performance could be observed based on these experimental data, indicating that the recuperator, despite having an increased total exchanged heat flux, is actually too small to exploit the full potential of the humidification. In a second step, by means of the SVR model, a first attempt was made to improve the accuracy and reduce the scatter on the recuperator performance determination. The predicted results with the SVR indicated indeed a reduced scatter on the determinations of the air mass flow rate and the amount of introduced water, opening a pathway toward online recuperator performance prediction. [DOI: 10.1115/1.4049266]

1 Introduction

To limit the effect of climate change, the United Nations (UN) has set a clear goal to reduce the global CO_2 emissions by 40% by 2030 [1]. To reach this goal, over the last years, the installed capacity of renewable energy (RE) production units has increased significantly [2]. This larger capacity leads to a significant increase in the RE power production in the total energy mix: e.g., in Belgium, Elia reported on a growth of 18% for the share of RE in the total mix from 2017 to 2018 (total share of 12% in the global mix for 2018) [3]. This larger share in RE is putting, however, a strong constraint on classical thermal power production, especially in centralized organized grids. Due to the intrinsic partially unpredictable and fluctuating nature of RE production (i.e., wind and solar), classical thermal production units need to provide the necessary flexibility to balance the grid. Shifting from large-scale centralized production to decentralized energy system (DES), possibly in combination with combined heat and power (CHP), offers a solution. In these DESs, flexible and reliable production from thermal units remains necessary, to compensate when not sufficient wind or solar power is delivered. Current battery technologies allow storage of RE power for a period of several hours to days, but seasonal storage is still a problem. Therefore, small-scale CHP units, like micro gas turbines (mGTs), will have a place in future DES production.

To really exploit their potential, the mGT has to become more flexible. The mGT is currently already (relative) fuel and operational flexible: the produced power can easily and fast be adjusted. Despite this flexibility, the main issue remains the fixed and constant heat-to-power ratio. In cogeneration applications, the mGT is typically linked with real users with real heat and electricity demands, which differ quite significant [4]. In example, domestic users have typically a high heat demand in winter and low in summer, while they present a rather constant power demand all year long, but highly fluctuating during the day. Given the relative low electrical efficiency of mGTs (30% for a 100 kW_e unit [5]),

[1]Corresponding author.

Manuscript received September 3, 2020; final manuscript received September 18, 2020; published online March 31, 2021. Editor: Jerzy T. Sawicki.

Copyright © 2021 by ASME

their operation in cogeneration applications remains heat driven. This includes thus automatically a shutdown in summer, leading to bad economic performance [4].

One way to decouple heat and power production in the mGT is applying cycle humidification. Cycle humidification, initially proposed on large-scale gas turbines (GTs) for power augmentation and NO_x reduction, allows to increase the specific power production and the electrical efficiency [6]. For large-scale GTs, the humid air turbine (HAT) cycle, which was first proposed by Rao [7] and uses a saturation tower and water recirculation loop for cycle humidification, was identified as the cycle with the highest performance [8]. Parente et al. were the first to apply this concept on the smaller mGT scale, leading to the development of the micro humid air turbine (mHAT) cycle [9]. When analyzing the optimal route for waste heat recovery and electrical performance increase using cycle humidification, the mHAT cycle was not identified by the authors of this paper as thermodynamically the best performing cycle with the highest efficiency increase [10]. Nevertheless, the cycle presents the best combination of optimal performance while keeping the layout rather simple [11], which is evenly important for small-scale applications.

Cycle humidification in mGT cycles has already been studied widely in literature and was summarized in a review [12]; however, the most important work on the mHAT is reported again below. The first to study the concept of mHAT were, as mentioned before, Parente et al. [9]. In their work, they studied the conversion of an mGT (range 100–500 kW_e) into an mHAT or mHAT-plus cycle, showing that both the efficiency (up to 3 to 5% absolute percentage points) and specific work (up to 50 to 70%) could remarkably be increased [9]. A similar study has been performed by Zhang and Xiao, investigating the off-design behavior of the mHAT. They reported a significant specific power and efficiency increase (3.7%), as well as a favorable off-design behavior [13]. Our research group [11], Nikpey et al. [14], and Majoumerd et al. [15] have studied the impact of converting the Turbec T100 (Malmö, Sweden) into an mHAT, by introducing a saturation tower. All indicated that without major changes to the cycle, the efficiency of the cycle can be increased from 30 to 33% at constant nominal power output [11,14,15]. Finally, our research group extended the steady-state analysis to a transient analysis, showing that during load steps, the ramp rates of the mGT need to be limited to avoid possible problems with compressor surge [16].

On the experimental side of the mHAT development, some research is available, however, only focusing on the global cycle performance. In the development process of the advanced humid air turbine plant, Hitachi (Tokyo, Japan) developed a specific 150 kW_e mGT [17] and equipped it with, next to the water atomizing inlet air cooling line, a HAT line capable of injecting up to 50 g/s of water to simulate the presence of a saturation tower in the cycle [18]. When operating with the HAT line, the power output of the unit was increased by 11 kW_e and the electrical efficiency by 2% points. When both water atomizing inlet air cooling and HAT lines were used during operation, 2.4%weight of water was added to the compressor air, resulting in a total efficiency increase of 3% points, while the electrical power output increased by 20% [18]. Wei and Zang also built and tested a small-size HAT test rig to characterize the off-design performance of the system, indicating a maximal efficiency increase of 3.1% points in wet mode [19]. The first full-scale tests of the mHAT have been performed by our research group [20–24]. First, a Turbec T100 mGT was equipped with a specifically designed spray saturation tower [25] and startup and shutdown procedures were determined [20]. Afterwards, the performance of the unit at constant power output [21,24] and constant rotational speed [23,24] was analyzed. Experimental results showed reduced fuel mass flow rate (4.3%) and increased electrical efficiency (relative increase of 4.8%) in constant power mode [21] and power output increases by more than 30% and overall electrical efficiency increases of up to 4.2% absolute points in constant speed mode [23,24]. Finally, most recently, Xu et al. built and tested a 100 kW_e mHAT test rig, presenting a 22.2% efficiency increase, when combining the mHAT with an aftercooler [26].

Although the potential of the mHAT has thus already been proven numerically and experimentally (and even economically [4,27]) for the full cycle performance, a detailed component performance analysis, especially of the recuperator, is still missing. As mentioned earlier by McDonald and Rodgers, high performance of the recuperator is essential to obtain high cycle performance for the dry mGT [28]. For the humidified case, the recuperator becomes even more important, as pointed out by the authors of this work when studying the energy and exergy fluxes in the mHAT [29]. So far, only a preliminary study was presented on the recuperator, discussing its possible degradation due to the humidification [30], without focusing on the performance itself. As pointed out by Pedemonte et al. [31] and Parente et al. [32], determining the relative humidity (degree of saturation) of the compressed air is challenging and cannot be done very accurate, since it is inevitable to have liquid droplets entering the cycle. Next to the knowledge on the amount of introduced water, accurate knowledge of the air mass flow rate through the system is needed as well to assess the total heat flux exchanged in the recuperator. This mass flow rate is typically not available.

Experimental assessment of the recuperator performance can thus only be done using indirect determination/calculation of the air mass flow rate and its water content, with possible low accuracy. Moreover, due to noise and measurement accuracy, online relative humidity and recuperator performance determination is challenging, given the large variation on all input variables, making control adjustments difficult. Nevertheless, direct, accurate, online monitoring of the recuperator performance would allow to assess the performance of the cycle during operation and will provide a tool to adjust the operating settings to optimize the humidification process and hence the electrical performance. In this framework, applying a support vector regression (SVR) model to assess the performance of the recuperator offers a solution.

In this paper, we present the assessment of the recuperator performance of an mGT under humidified conditions using experimental data extended with a preliminary analysis using a SVR model to study the possibility of rendering out part of the measurement noise, thus to increase the prediction accuracy. First, the cycle layout and the specific importance of the recuperator is repeated, followed by a description of the test rig and used measurement procedure. Next, the experimental analysis of the recuperator and global cycle performance under humidified conditions, using average measurement data taken over a large period, is presented. Additionally, the SVR model is explained and applied on one specific dataset. By presenting this model, we aim to show the potential of SVR models for accurate instantaneous, online, recuperator and cycle performance assessment. Finally, a conclusion and future work are presented.

2 Dry and Humidified Microgas Turbine Cycles Description

The considered mGT used for the analysis presented in this paper, the Turbec T100 (now AE-T100), operates according the recuperated Brayton cycle. The cycle consists of (black parts in Fig. 1): a variable speed centrifugal compressor, to compress the incoming fresh air to approximately 4 bar; a recuperator, to preheat the compressed cold working fluid using heat from the flue gases; a counterflow can burner, where natural gas is burnt to heat the working fluid to the maximal allowable turbine inlet temperature (TIT) of 950 °C and a radial turbine, over which the flue gases expand, delivering the mechanical power to drive the compressor and the high speed permanent magnet generator for electrical power generation (the high-frequency electrical power is then converted in the power electronics and injected in the grid). Since the Turbec T100 is a cogeneration unit, the remaining heat from the flue gases is recovered and transformed in thermal power (hot water) in the economizer. At nominal power output (100 kW_e and

160 kW_{th}), the unit has an electrical efficiency of 30% and a total efficiency of 80% at standard inlet air conditions [5].

The T100 is standard equipped with two control loops. The first loop allows the engine to operate at constant produced electrical power. Different from large-scale GTs, the mGT does not operate at constant rotational speed. So rather than changing the inlet air mass flow rate using inlet guide vanes or changing the TIT for power control, the control system will, depending on the requested power output, vary the rotational speed and thus the air mass flow rate. The variable operational speed control allows to keep the compressor operating at or close to its nominal isentropic efficiency, leading to better part load performance. Moreover, varying the rotational speed to control the electrical power output preserves a rather constant surge margin for the compressor, as was previously presented in Ref. [33], and thus leading to a better protection of the compressor. The second control loop aims at keeping the TIT close to the maximal value, by keeping the turbine outlet temperature (TOT) constant at 645 °C by changing the fuel mass flow rate injected in the combustion chamber. In doing so, the efficiency of the unit can be kept rather high, even when operating at part load (minor efficiency correction of 0.93 at 50% of the nominal load [5]).

The mGT cycle is converted into an mHAT by adding a saturation tower in between the compressor outlet and the recuperator inlet (grey parts in Fig. 1). In this saturation tower, an excess of hot water, coming from the economizer, is brought into contact with the hot compressed air. The compressed air is then humidified through the evaporation of a fraction of this water (approximately 5%). The necessary energy to complete the evaporation—evaporation heat—is partially provided by the sensible heat of the hot compressed air, but mostly by the sensible heat from the hot water. Indeed, leaving the saturation tower, the hot water has a lower temperature than when entering the component. The outgoing water is then heated again in the economizer. Through this process, the thermal power of the economizer, which is lost in case there is no demand for heat, is partially recovered and reintroduced in the cycle, leading to better cycle performance.

Cycle humidification leads indeed to higher electrical performance of the mGT. Introducing water in the mGT cycle after the compressor allows to reduce the compressor work, while keeping the turbine mass flow rate and thus also the turbine power constant, leading to an increased specific power and net power output when operating at constant rotational speed. Moreover, as a result of the water introduction (liquid, steam or by means of a saturation loop), the recuperator cold side inlet temperature will reduce. This temperature reduction, in combination with a higher heat capacity (increased water fraction), allows for more heat recovery and thus also a higher electrical efficiency. Indeed, while performing an energy and exergy analysis of the mGT and mHAT cycle, using Sankey and Grassmann diagrams, our research group was able to identify that in terms of exergetic performance, the action of the saturation tower in the mHAT actually leads to a decrease of the exergetic content of the working fluid (a net exergy destruction) [29]. This destruction is the result of the lower temperature of the working fluid after humidification. Although the saturation tower itself does not contribute to a higher exergetic flow rate of the humidified compressed air, it actually enables the recuperator to increase its performance. Indeed, inside the recuperator, a higher energy and exergy exchange between the flue gases and the humid compressed air is observed, leading to an increased outgoing exergy and energy flow [29]. This clearly highlights that cycle humidification, with as aim an improvement of the electrical performance of the mGT, only makes sense if the humidification (water introduction) occurs before the recuperator, where it will lead to a higher waste heat recovery. This was indeed already confirmed in literature by several researchers, including the authors of this paper: i.e., introduction of water or steam in the combustion chamber (so behind the recuperator) leads to higher electrical power output, but at the cost of a higher fuel flow rate and thus lower electrical efficiency [10,34,35].

The action of the recuperator is thus clearly essential for the mHAT performance improvement. Therefore, correct assessment of the recuperator performance (effectiveness and exchanged heat flux) is, as mentioned in the introduction, essential to allow for a correct prediction of the global humidified cycle performance [35].

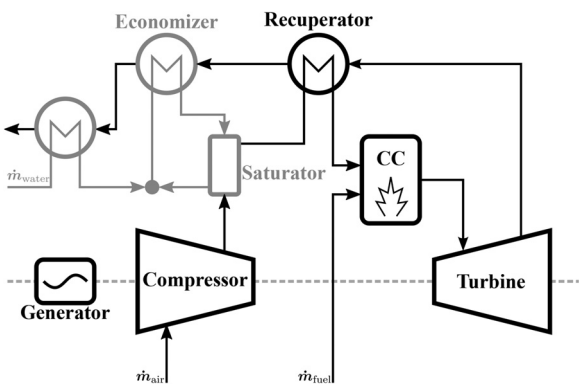


Fig. 1 The standard mGT, operating according to the recuperated Brayton cycle (black parts), is converted in an mHAT by adding a saturation tower and water recirculation loop in between the compressor outlet and the recuperator inlet (grey parts)

3 Experimental Recuperator and Cycle Performance Analysis

In this section, first the experimental setup is discussed, followed by the experimental determination of the recuperator effectiveness and exchanged flux and finally the global cycle performance, all based on measurements. The problem related to the accuracy on the determination of the air mass flow rate and the amount of evaporated water entering the cycle is highlighted for each parameter.

3.1 Test Rig Description. The test rig used for the analysis presented in this paper is the Turbec T100 mGT test rig of the Vrije Universiteit Brussel (VUB). The test rig description can be found in Refs. [20] and [24], but the main features, important for the analysis presented in this paper, are repeated below.

The test rig consists in a Turbec T100 version 2 mGT and an integrated spray saturation tower, without packing material to limit the additional pressure loss [25], with water circulation loop. Due to space limitation, the saturation tower was placed next to the mGT rather than on top of the machine, closer to the compressor outlet and recuperator inlet (Fig. 2), leading to significant additional pressure and heat losses. A bypass valve was also installed to bypass the saturation tower, allowing to run the mGT in its original configuration (black cycle from Fig. 1). Finally, the mGT test rig was equipped with pressure, temperature, mass flow, and O_2 exhaust sensors to assess the impact of water introduction on the different components of the cycle and the global performance. A complete overview of all installed sensors and their accuracy can be found in Ref. [24], together with a schematic representation of the cycle, indicating all specific valve and sensor locations.

To measure the air flow rate in the system, typically a mass flow sensor is installed between compressor outlet and recuperator inlet. Due to practical limitations (need to limit pressure losses in the cycle to avoid the compressor from going into surge), no air mass flow meter could be installed. In addition, for budgetary reasons, no such sensor could be installed either. Direct determination of the amount of evaporated water entering the cycle by taking the difference between the in- and outgoing water flow rate

of the saturation tower is also no option: the evaporated amount, typically 5% of the total injected mass flow rate (2.5 kg/s for nominal operation), is actually below the measurement accuracy (typically 1 to 2% of the reading per water flow meter).

The data used for the analysis of this paper are obtained over a period ranging from 2012 till 2019. Each of the individual points, shown in Secs. 3.2 and 3.3, is obtained using the measurement procedure described in Ref. [20] and is taken at constant power output and constant TOT, using the control system as described in Sec. 2, or at constant TOT and constant rotational speed. Indeed, for some specific previously reported humidified tests [24], the original control system was slightly modified, allowing the mGT to operate at constant rotational speed rather than at constant power output. As presented previously by the authors of the paper [24], applying cycle humidification in constant speed mode has a slightly different impact on the cycle than applying it in constant speed mode. However, when looking at the recuperator alone, this difference is negligible. Hence, we opted not to distinct the results obtained at constant rotational speed or constant power output. Moreover, since the test rig is equipped with bypass and bleed valves, five different operating regimes are distinguished:

- *Original*: Data taken on the original T100 test rig, before implementation of the saturation tower in the cycle;
- *Bypass*: Dry operation of the mGT with the bypass over the saturation tower open (recuperated Brayton cycle, no air passing through the saturation tower);
- *NoBypass*: Dry operation with the bypass valve over the saturation tower closed, compressed air passing through the saturation tower (without water injection);
- *Bleed*: Similar operation as NoBypass, but with a small air bleed between compressor outlet and saturation tower inlet;
- *Inject*: Operation in humidified mode, with water injection in the saturation tower (and air bleed for surge margin increase, see later).

Although the performance of the mHAT was already validated experimentally by the authors of this paper [21,24], there are still some uncertain points: e.g., the amount of air bleed is not known (see later), nor the actual humidity level could be determined. Additionally, so far, when assessing the impact on the global performance, as reference data, a specific run was performed on the same day, which is rather inconvenient and time consuming. The analysis presented in this paper aims thus to reduce these efforts, by providing an accurate determination of the air mass flow rate and evaporated water amount, allowing for correct recuperator effectiveness and more general global cycle performance assessment.



(*a*) (*b*)

Fig. 2 Pictures of the integration of the saturation tower in the mGT cycle in between the compressor outlet and recuperator inlet (*a*) and of the saturation tower with circulation pump, valves, and sensors (*b*)

3.2 Experimental Recuperator Performance Analysis. A first parameter to assess the recuperator performance is the heat exchanger effectiveness. To determine this effectiveness, all four temperatures of the in- and outgoing flows were measured, using additionally installed sensors in the recuperator cold side in- and outlet (combustor inlet temperature (CIT)) and the hot side outlet. The temperature sensor used for the TOT control was used to measure the hot side inlet temperature. The effectiveness is calculated as follows:

$$\eta_{\text{rec}} = \frac{\max(\text{CIT} - T_{\text{rec,cold,in}}, \text{TOT} - T_{\text{rec,hot,out}})}{\text{TOT} - T_{\text{rec,cold,in}}} \tag{1}$$

When considering the recuperator as adiabatic, $\Delta T_{\max}$ is normally found on the cold side of the heat exchanger. However, due to the heat losses in the actual engine, for all different operating regimes of the mGT, $\Delta T_{\max}$ is found on the hot side instead.

The recuperator effectiveness is a function of the mass flow rate going through the system. However, as mentioned before, this mass flow rate was not measured. As alternative, effectiveness is plotted as function of the generated electrical power output (Fig. 3(*a*)) and the corresponding rotational speed (Fig. 3(*b*)), set by the control system to keep the power output constant. Each of the datapoints represents the average data of an mGT run performed at constant power output, during a period ranging from 15 min up to 3 h, depending on the purpose of the performed test (valid for all datapoints presented in the different figures in this paper). Although the mGT operates thus at constant power output and not at constant rotational speed, given that the boundary and inlet conditions remained relative constant during this period, the rotational speed set by the control system also varies only limited.

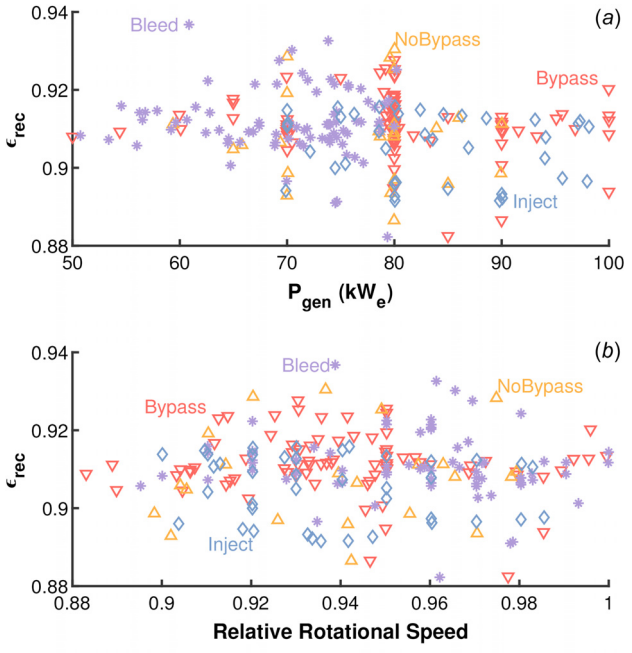


Fig. 3 The recuperator effectiveness does not present a clear trend for any of the dry operating regimes (Bypass, NoBypass, and Bleed) as a function of generated electrical power (*a*) or its corresponding rotational speed (*b*) due to the large scatter on the air mass flow rate. Under humidified conditions (Inject), the recuperator presents a slight reduced effectiveness.

The effectiveness of the recuperator in the original configuration could unfortunately not be assessed, since the temperature sensors to measure CIT and the recuperator hot side outlet temperature were only installed when the saturation tower was integrated in the cycle.

In contrast to what was expected, there is no noticeable variation or clear trend in the recuperator effectiveness depending on the produced electrical power (Fig. 3(*a*)), nor on the rotational speed (Fig. 3(*b*)), even though effectiveness is a function of the recuperator mass flow rate. An explanation can be found in the different mass flow rates passing through the recuperator, even at constant power output or rotational speed, due to different inlet air temperature and heat losses (see later). The values present a rather larger scatter, ranging from 88% to 93%, which is comparable with the values presented by the manufacturer of the recuperator: design values range from 92% at the lowest cell mass flow rate down to 88% [36]. Comparison of the obtained effectiveness for the different operating regimes shows a small negative difference between the dry operation (Bypass, NoBypass, and Bleed cases) and the humidified operation (Inject case). Indeed, generally, the effectiveness in the humidified case is slightly lower, indicating that the humidification has a minor negative effect on the potential heat recovery in the heat exchanger (approximately 1 to 2% lower).

Although the effectiveness is a good indicator for the performance of the recuperator, the main improvement of the mHAT cycle, as discussed in Sec. 2, is found in the higher total exchanged heat flux in this heat exchanger. The lower effectiveness in the humidified case only reflects that the current used recuperator is actually too small for the wet cycle. Indeed, in the wet cycle, given the significant increase in the heat capacity of the working fluid, a larger total heat flux is available and could thus be exchanged. Since the surface of the recuperator is fixed and optimized for the dry operation, in the wet case, only a smaller temperature increase/decrease could be obtained as a result of the higher heat capacity. This leads to a smaller numerator in Eq. (1) compared to the available maximal potential (denominator in Eq. (1)), which increases due to the lower cold side inlet temperature as a result of the humidification in the saturation tower. A redesign of the recuperator (larger heat exchange surface) would thus allow for a further improvement of the total wet cycle performance.

To assess accurately the exchanged heat flux, recuperator mass flow rate and flow composition (water fraction) are needed. As mentioned before, direct measurement of both parameters was not possible on the considered installation, requiring thus an indirect assessment, by using the compressor map (using the rotational speed and the compressor outlet pressure) and the remaining O_2 fraction in the exhaust gases in combination with the measured injected fuel mass flow rate.

The first step toward the recuperator heat flux determination involves the determination of the mass flow rate through the cycle, starting by determining the compressor operating point (Fig. 4). This point can be determined based on the measurements of the rotational speed and the pressure at compressor outlet, in combination with the available data from the manufacturer [37]. Although both rotational speed and compressor outlet pressure can be measured accurately (typical optical rotational speed and differential pressure sensors have accuracies of 0.01%), there is still some uncertainty on the used compressor map, as previously highlighted by Zanger et al., when analysing the surge margin of the T100 [38]. Since the uncertainty on the compressor map cannot be assessed, it is thus not possible to indicate the uncertainty on the obtained compressor air mass flow rates.

When looking at the specific operating point of the mGT, the five different operating regimes can clearly be identified and distinguished (Fig. 4, original datapoints in (*a*), and their corresponding linear trendline in (*b*)). The original operating line (Original, green circles/line) shows the compressor working point before applying the modifications to the cycle, i.e., introduction of the

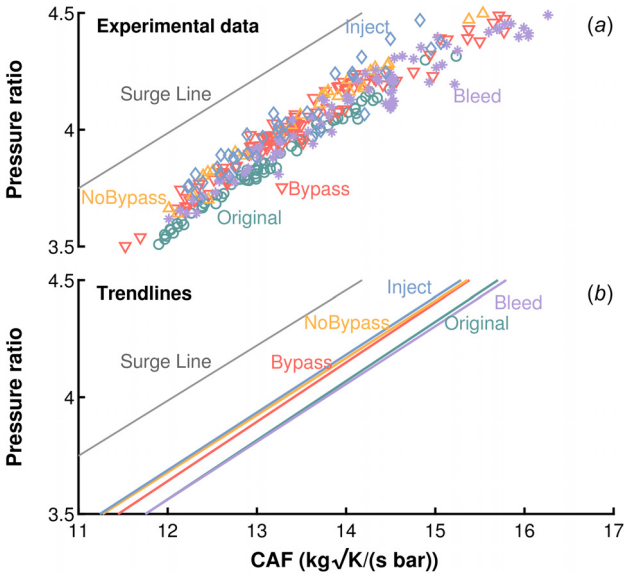


Fig. 4 The different operating regimes result in distinct compressor operating lines (original datapoints in (*a*), and their corresponding linear trendline in (*b*)) when the mGT is operated in constant power mode, depending on additional pressure losses (shift to left compared to the Original operating line, Bypass, and NoBypass), air bleed (shift to right at higher power outputs, Bleed), or water introduction (shift to left, Inject)

saturation tower. As mentioned in the introduction, the mGT operates at constant power. This includes that the mGT control system changes the compressor operating point by adjusting the rotational speed, rather than keeping this speed constant (and operating thus along a constant speed line). This allows to keep the surge margin constant, while operating at relative high compressor efficiency (even at part load).

After the integration of the saturation tower in the cycle, a clear, constant shift in operating point can be observed (Bypass, red reversed triangles/line in Fig. 4). Although a bypass with valve was installed, allowing to bypass the saturation tower, the gas path has been changed significantly (longer tube length and additional valve to close the bypass, Fig. 2(*a*)). This leads to an additional, rather constant, pressure loss of on average 4% over the piping system for the full operating range (50 to 100 kW_e). The additional pressure loss forces the compressor to change its operating point toward higher pressure ratios and thus smaller surge margin. Indeed, an average reduced surge margin from 12.3% (Original) to 10.2% (Bypass) is observed over the full operating range. The surge margin (SM) is defined as

$$\mathrm{SM} = \frac{\dot{m}_{\mathrm{comp,working}} - \dot{m}_{\mathrm{comp,surge}}}{\dot{m}_{\mathrm{comp,working}}}.100\% \tag{2}$$

where $\dot{m}_{\mathrm{comp,working}}$ is the air flow rate at the working point and $\dot{m}_{\mathrm{comp,surge}}$ is the air flow rate at the surge limit (the same definition was used in Ref. [33]). As surge limit, the experimentally validated surge line found by Zanger et al. was used [38]. Closing the bypass over the saturation tower, introducing thus an extra component (the saturator) and thus extra pressure loss, shifts the operating point even closer to the surge limit (NoBypass, yellow triangles/line in Fig. 4, SM equal to 9.5%).

Water introduction in the mGT behind the compressor leads to a competition between the air and water, since the total mass flow rate going through the cycle is determined by the turbine operating point. Adding an additional amount of water behind the compressor by means of evaporation leads thus inevitably to a reduced compressor air mass flow rate and thus a reduced surge margin (as

previously presented in Ref. [33] by the first author of this paper, when presenting the impact of steam injection on this machine). Since water injection leads to a reduced compressor surge margin, in combination with the extra pressure losses induced by the entire injection unit (saturation tower and extra piping), for safety reasons, each of the wet test was performed with a small air bleed.

The action of this air bleed, in dry operating conditions, is visible on the compressor map (Bleed, purple stars/line in Fig. 4), showing the significant surge margin increase. On average, applying an air bleed leads to an SM increase from 9.5% (NoBypass case) to 12.6% (Bleed case, which is equal to the Original surge margin). As previously mentioned by the authors of this paper [24], this air bleed mass flow rate could unfortunately not be measured. Moreover, the specific type of valve used—globe valve—did not allow for an accurate valve opening section determination. So the option to calculate the flow rate based on the choking constants was unfortunately also not possible. The authors of this paper were capable to obtain an estimate of the valve opening based on the comparison of the experimental measured performance with simulations, indicating that the valve opening is approximately 22 cm^2 [24]. Nevertheless, this value has some uncertainty. Hence, it was decided to not use the valve opening to determine the air bleed mass flow rate. Since this air bleed mass flow rate is not measure, nor calculated directly, assessment of the mass flow rate based on the compressor operating point required extra calculations (see later). Finally, due to the water injection, the operating point shifts again to the surge line (Inject, blue diamonds/line in Fig. 4, reduced SM of 9.2%).

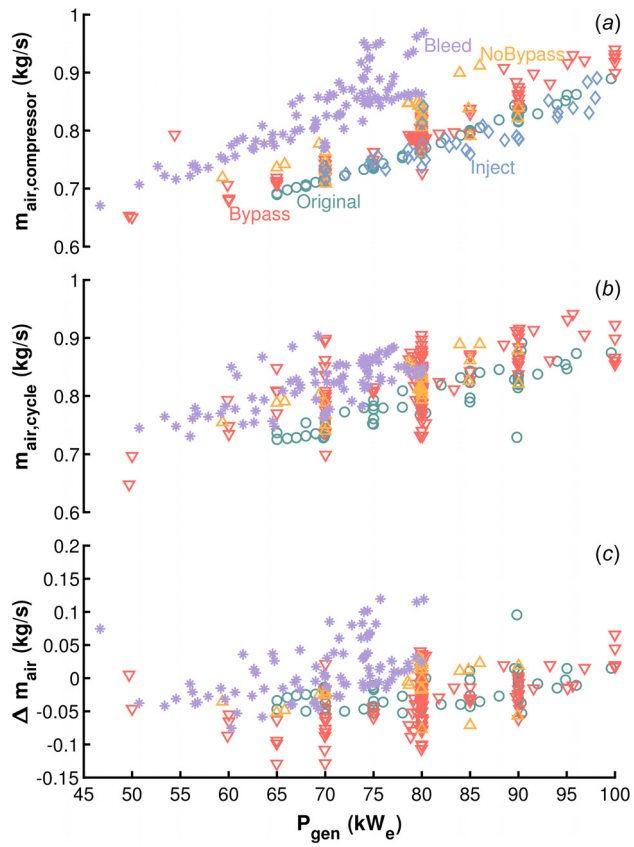


Fig. 5 Due to the variable operational speed, the air mass flow rate going through the compressor (*a*) and cycle (*b*) increases with increasing electrical power output when operating in dry mode. The action of the air bleed is clearly visible when comparing the air mass flow rate through compressor and the cycle (Bleed case). Finally, due to the uncertainty on the different measurements, using the compressor map (*a*) or the exhaust gas composition (*b*) to determine the air mass flow rate shows some differences (*c*).

Based on the compressor operating point, the compressor air flow rate was calculated (Fig. 5(*a*), $\dot{m}_{air,comp}$). Depending on the operating mode (operation without air bleed), this mass flow rate corresponds to the mass flow going through the recuperator. As expected, due to the action of the control system, higher requested power output leads to higher compressor air mass flow rate. Except for the results of the original configuration (Original), the obtained mass flow rates show a rather large scatter. This scatter can partially be explained by the different inlet air temperatures during the different experiments—especially at 70 and 80 kW_e, since at these operating points, most of the measurements were taken over the years (during both summer and winter time), but mostly by the additional different heat losses (see Sec. 3.3). Overall, the mass flow rate increases with increasing power output. The additional pressure loss resulting from the modified cycle for the Bypass and NoBypass leads to higher mass flow rates at constant power output. The higher mass flow rate is needed to compensate for these pressure losses when operating at constant electrical power. When applying an air bleed, obviously, an even higher air mass flow rate goes through the compressor (Bleed). Finally, when injecting water at constant power output, this mass flow rates is decreasing again (Inject).

In an attempt to assess the amount of air bleed, the air mass flow rate through the system was calculated using the measurement of the wet O_2 content of the flue gases together with the measured fuel mass flow rate and assuming complete combustion. A similar procedure was used by the authors and presented in Ref. [33] to determine the dry and wet compressor operating point under steam injection conditions. The results (Fig. 5(*b*), $\dot{m}_{air,cycle}$), although having a significant uncertainty (approximately 4% [33]), confirm the same trends and observations as discussed in previous paragraph. There is, as presented in Fig. 5(*c*), $\Delta\dot{m}_{air}$, indeed a small discrepancy between the air mass flow rate determined using the corrected air flow and the determination using the wet O_2 content of the flue gases. Nevertheless, by assessing the general trend of the results when applying an air bleed, the air bleed fraction as function of compressor outlet conditions—temperature and pressure—could be determined. This fraction is necessary to be able to calculate the water content in the humidified case, since the O_2 content of the flue gases is measured on wet basis.

Since a constant air bleed opening was used throughout the wet and dry tests, based on the calculated air bleed in the dry case and considering the bleed stream as choked, the air bleed mass flow rate in the wet case could be determined as well. Once this air bleed is known, the amount of injected water and corresponding relative humidity of the working fluid under humidified operation could be calculated (Fig. 6), using the calculated compressor mass flow rate in combination with the measurement of O_2 content of the flue gases and the fuel mass flow rate. Additionally, only the operating points with a nominal water injection of 2.5 kg/s in the saturation tower are presented. A reduced water injection flow rate in the saturation tower only leads to partial humidification and thus compressor air entering the recuperator that is not fully saturated.

The amount of water entering the cycle through evaporation in the saturation tower ranges between 40 and 60 g/s and increases, as expected, with increasing electrical power output (Fig. 6). For most of the cases, the relative humidity of the air entering the recuperator is equal to or even exceeds 100% (even 200% in some of the cases). This indicates that the amount of water entering the mGT working fluid is higher than the amount that would be expected to evaporate in the saturation tower. Indeed, depending on the requested power output, a value between 30 g/s (70 kW_e) and 40 g/s (100 kW_e) is expected, based on our validated Aspen® simulations.[2] The tests resulting in very high water introduction—more than 40 g/s—correspond to a relative humidity of more than 100% (Fig. 6(*b*)), which is obviously not feasible. These results

[2]More information about the Aspen® simulations and the validation can be found in Refs. [21], [23], [24], and [39].

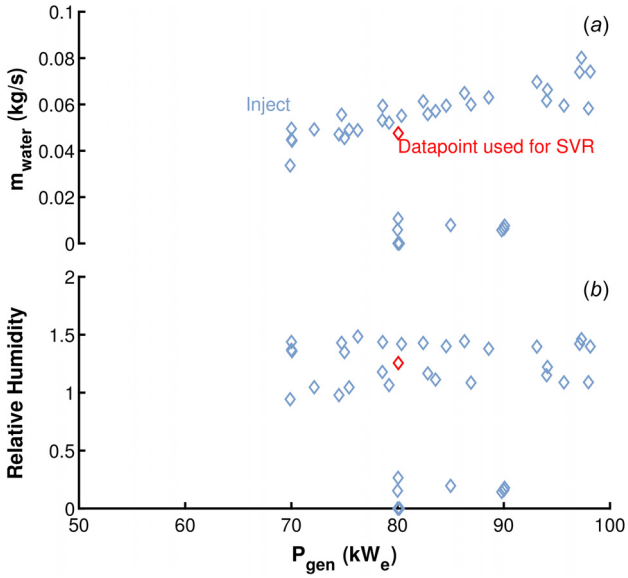


Fig. 6 The calculated introduced water mass flow rate in the mGT cycle working fluid (*a*) allows determination of the relative humidity of this working fluid (*b*) when exiting the saturation tower. The relative humidity of 100% for some experiments confirm complete saturation of the working fluid, while the values above 100% indicate that during these test, a significant amount of liquid water was also entering the working fluid, explaining the too high relative humidity.

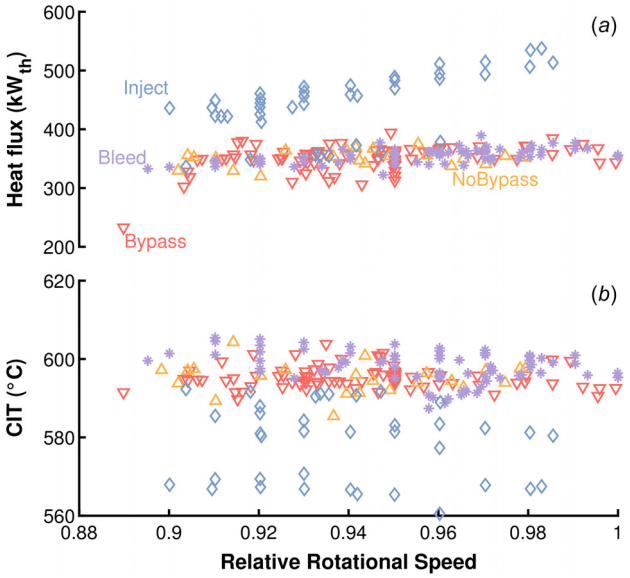


Fig. 7 The calculated exchanged heat flux (*a*) in the recuperator shows, as expected, a much higher exchanged flux in the humid case (Inject) as the result of the lower temperature at the cold side recuperator inlet in combination with the higher water content of the compressed air and flue gases (higher heat capacity). The lower cold side outlet temperature CIT in the humid case (inject) indicates that the performance can be increased further by using a large heat exchanger.

clearly indicate that in this case, liquid water is entering the recuperator. This hypothesis could be confirmed by a significant reduction of the temperature at the cold outlet of the recuperator in the lower part during startup (problem reported by the authors of this paper in previous work [24]), the lower CIT for all humidified case (see Fig. 7(*b*)) and by a visible observed liquid film in the piping behind the saturation tower, through the installed sight glass.

Finally, for all different cases, the exchanged heat flux over the heat exchangers could be calculated (Fig. 7(*a*)). The results show a large scatter of the different dry cases (Bypass, NoBypas, and Bleed), without any significant trend. Additionally, since the air mass flow rate for all dry and wet cases and the amount of evaporated water entering the cycle for the wet case had to be calculated using several other measurements and models, there is some significant uncertainty on the final results for the air mass flow rate, explaining the scatter on the results. As mentioned before, the uncertainty on the air mass flow rate determination using the measurement of the O_2 content in the flue gases amounts 4% [33]. Moreover, since the accuracy of the compressor map is not known, it is not possible to assess the uncertainty on the air mass flow rates obtained using this map. This highlights again the importance of accurate data for recuperator performance assessment.

The expected higher flux under humidified operation can clearly be observed (increase of more than 50% between the humid case Inject and all dry cases Bypass, NoBypass, and Bleed, Fig. 7(*a*)). This higher flux is, as discussed before, a result of the lower cold side inlet temperature as a result of the humidification and the favorable heat capacity due to the presence of the injected water. Analysis of the cold side outlet temperature (CIT, Fig. 7(*b*)) indicates that the heat flux can be increased even further. Indeed, in all cases, the hot side inlet temperature is constant and equal to 645 °C due to the control system (operation at constant TOT). In the dry cases, the recuperator operates with a hot inlet, cold side outlet temperature differences of 50 °C, while this is lower in the humid case (Inject, which was also reported when explaining the lower recuperator effectiveness). For optimal mHAT performance, it would be interesting to increase the recuperator size (heat exchange surface) to obtain a similar CIT as in the dry case. This will reduce the necessary fuel flow rate further and allowing to exploit the full potential of cycle humidification.

3.3 Experimental Global Cycle Performance Analysis. In addition to the recuperator performance, the global performance of the system in the different operating regimes was also determined (Fig. 8). To exclude the influence of the requested power output and the compressor inlet air temperature, who both have an influence on the mGT electrical performance, the obtained electrical efficiencies (Fig. 8(*a*)) were normalized using the correction factors for part load, published by the manufacturer of the engine and the reference efficiency for operation at nominal power output at different inlet air temperature [5]. The reported corrected efficiencies show that even in the original configuration, the efficiency is lower than presented by the manufacturer (normalized efficiencies are all below 1, Fig. 8(*b*)). Especially at part load, the mGT of the VUB is under-performing. According to the manufacturer, the mGT should present higher efficiencies at part load than at nominal load (indicated correction factor is above 1 in Ref. [5]). However, this trend was never observed before on this specific test rig and already reported before by the authors of this paper in Ref. [40], where a rather linear decreasing efficiency, as is the case here, was observed.

The impact of the additional pressure losses, and in addition the air bleed, leading to lower cycle performance, can clearly be seen in the electrical efficiency (Fig. 8). The cases with air bleed (Bleed) present the lowest electrical efficiency. Moreover, the extra pressure loss, and loss through the bleed, requires the control system to increase the operational speed. The requested increase is however above the allowed maximal rotational speed at the specific operating point (requested power output), explaining the lack of data at high power output (above 80 kW_e).

The large scatter observed for the dry operation with bypass (Bypass case) or without (NoBypass case), even after correction, originate from the heat losses induced in the system through the longer gas path, that are not accounted for in the correction.

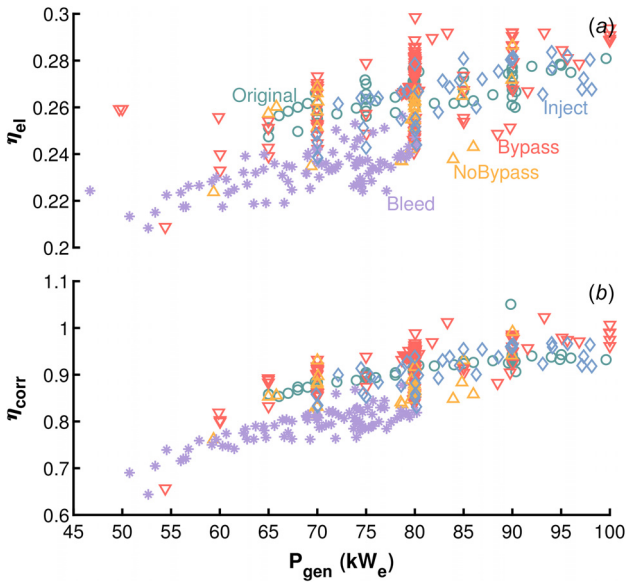


Fig. 8 While the air bleed (Bleed case) has a clear negative effect on the absolute (*a*) and corrected efficiency (*b*) in dry operation, when compared to the Original case, less impact of the additional pressure losses (Bypass and NoBypass cases) can be observed. Applying cycle humidification (Inject case), increases the electrical efficiency, compensating for pressure and bleed losses, bringing the efficiency back to the initial levels.

Indeed, these heat losses depend on the atmospheric conditions and the operation of the ventilation of the room of the T100 and are thus not considered in the correction. In the Original dry case, a similar scatter is observed when only looking at the efficiency of the engine, but after correction, the scatter has been removed, since the influence of the inlet air temperature was removed. The original mGT has only a short gas path between compressor outlet and recuperator inlet, leading to negligible heat loses.

Finally, with water injection (Inject), the efficiency can be increased, compared to the case with air bleed (Bleed). Indeed, since water injection always occurs with an air bleed (for safety reasons), to assess the positive impact of cycle humidification, the results must be compared with dry results with air bleed. Humidifying the working fluid even allows to bring the electrical efficiency back to the level obtained before the modifications (Original). If a larger recuperator would be used, this efficiency could be increased further, as discussed in Sec. 3.2. The scatter in the results is, as mentioned before, a result of the different humidification levels in the different cases as well as the different amount of liquid water entering the recuperator. Especially the water injection cases at 80, 85, and 90 kW_e, corresponding to a relative humidity close to 100%, show a maximal efficiency. For the analysis presented in Sec. 4, data obtained at 80 kW_e with a relative humidity of 125% are used.

4 Support Vector Regression Analysis

Support vector regression models are rigorous surrogates used in engineering design space exploration and optimization, due to their better handling of the curse of dimensionality [41] and improved performance under the presence of noise. On the contrary, SVR models do not provide variance for their predictions, while their performance is heavily dependent to their configuration. The latter issue breaks down to a parameter estimation problem, where three hyper-parameters are subject of optimization. Furthermore, the parameters control the tradeoff between the empirical error and the complexity of the prediction response, the threshold for which the estimation error is ignored and the width of the basis function used for prediction. For a detailed analysis of the mathematical structure, the reader is referred to Smola and Schölkopf [42]. It is understood that the use of SVR models necessitates the accurate definition of the parameter mentioned above.

To this end, exhaustive grid search [43], analytical methods [44], and optimizers [45–47] are employed in the literature to identify the proper parameters set. The first two methods represent the extremes of the cost-speed tradeoff, providing either very accurate but costly techniques (exhaustive grid search) or less accurate but ultrafast methods (analytical methods). In the current study, a classic genetic algorithm is used [48], since optimization can identify parameters that lead to sufficiently good prediction accuracy in less computational time than an exhaustive grid search. Moreover, the classic genetic algorithm is enhanced by a randomization search term, activated when stagnation in convergence is suspected [49].

The output parameter set is then used to configure an SVR model and train it using a specific dataset. In this paper, the SVR model was applied on the time series of one specific dataset. This dataset was taken at constant electrical power operation (80 kW_e). According to the experimental analysis, presented in Sec. 3.2, during this test, 47.5 g/s of water was entering the cycle through evaporation in the saturation tower, leading to a relative humidity of 125% (red point on Fig. 6). Presenting the calculated instantaneous air mass flow rate (presented by the black triangles, Fig. 9) for this dataset over time highlights again the problem. Noise and measurement accuracy lead to significant scatter on the data, justifying the use of an SVR model. One can argue that the noise on the signal can be reduced by filtering as well. However, when using the data in an online monitoring and optimization framework, as is the perspective of this and future work, filtering is not optimal. Indeed, once the SVR is trained, it can be used all the time, while when applying filtering, it needs to be applied continuously, which is time and calculation costly. Moreover, filtering offers no solution for the lack of accuracy.

In this paper, the SVR model is thus used in an operational monitoring setting, using two output quantities (air mass flow rate $\dot{m}_{air}$ and introduced water amount $\dot{m}_{water}$) in combination with seven input variables, being compressor inlet ($T_{comp,in}$) and outlet temperature ($T_{comp,out}$), compressor outlet pressure ($p_{comp,out}$), fuel mass flow rate ($\dot{m}_{fuel}$), rotational speed (N), generated electrical power (P_{gen}), and wet O_2 content of the flue gases ($O_{2,flue\,gas}$). These parameters are the same parameters that were used in the experimental approach to assess the air mass flow rate and corresponding amount of introduced water, presented in Sec. 3. All quantities are taken with respect to time, with a sample frequency of 1 s over a time period of 45 min. The aim of this analysis was to create a surrogate that captures the dynamic response of the output considering the changes of the input variables in this time interval, reducing the scatter on the time series. Both air mass

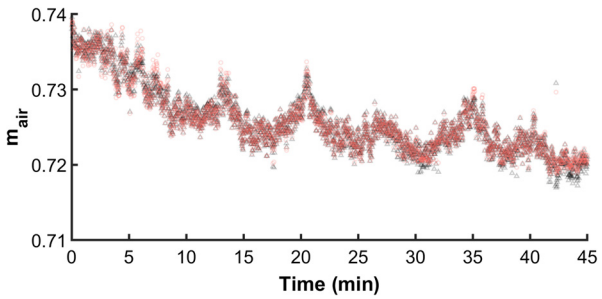


Fig. 9 Time series of the measured air mass flow rate (black triangles) and predicted results using the SVR model (red dots) show the potential of the model to reduce scatter and improve accuracy

Table 1 Standard deviation values for the model predictions, corresponding to the different input parameters as demonstrated in Fig. 10

Input parameter	P_{gen}	N	$T_{comp,in}$	$T_{comp,out}$	$p_{comp,out}$	$\dot{m}_{fuel}$	$O_{2,flue\ gas}$
σ	0.00420	0.00164	0.00372	0.00398	0.00268	0.00333	0.00249

flow rate and introduced amount of water are considered as the target outputs.

To assess the SVR model, first the response of the output (here air mass flow rate, but similar results are observed for the amount of introduced water) are plotted as function of all input variables (black triangles, Fig. 10). These plots show a large scatter, even when considering the mGT was operated at constant power output. For the rotational speed, as expected, a rather linear trend can be observed, similarly for the compressor outlet pressure and O_2 content of the flue gases, although here a large scatter is observed. For the other parameters, e.g., inlet air temperature and the power output, no real trend is observed. After creating the surrogate model, the predicted output is plotted again against the input parameters (red dots). Indeed, the predictions of this SVR model allow to reduce this scatter for all quantities. For each of the parameters, the standard deviation values for the predicted output are reported in Table 1.

Finally, comparison of the predictions over time (red dots, Fig. 9) with the direct calculated values (black triangles) shows again the improvements made by the model. To provide a more

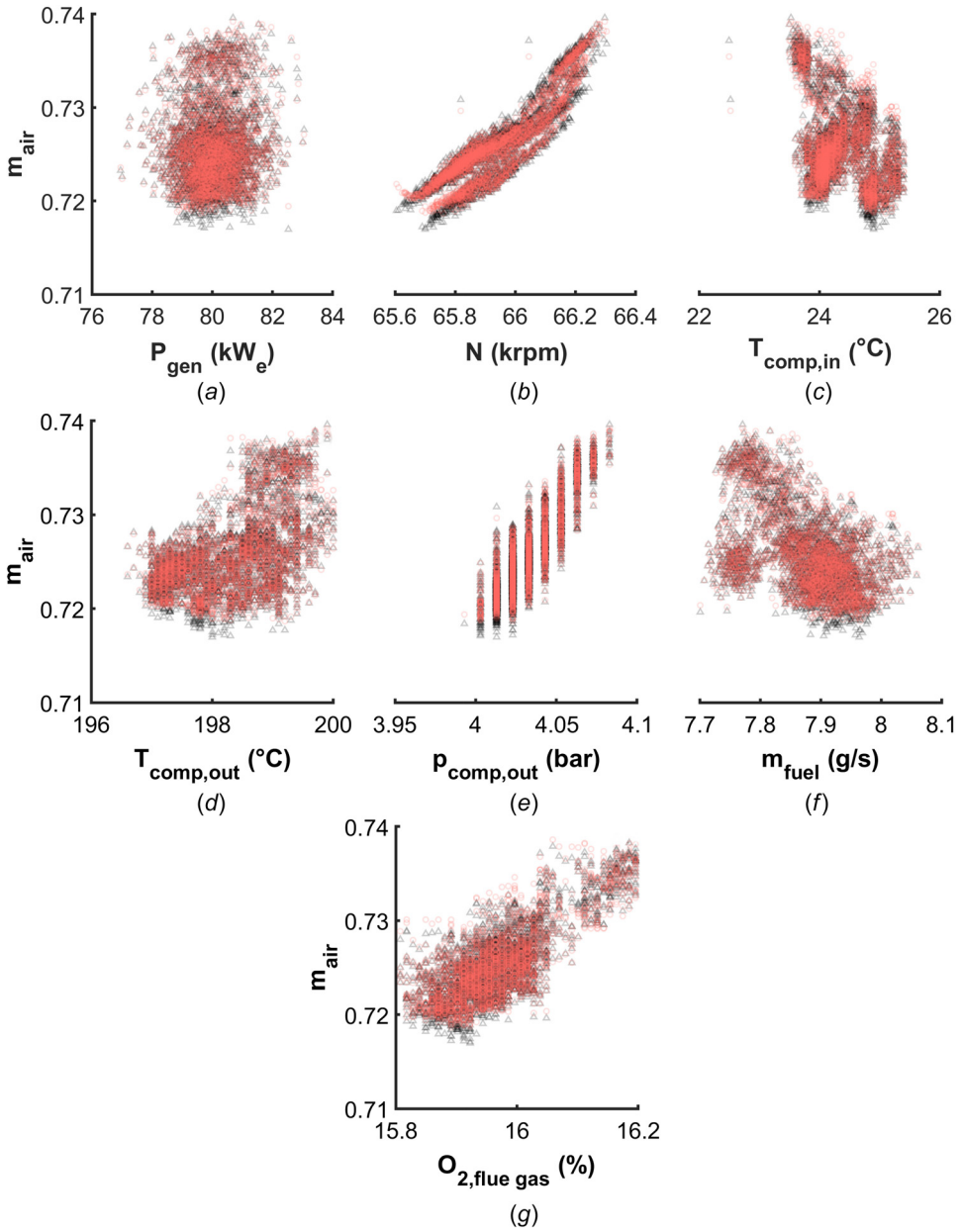


Fig. 10 Surrogate model allows to reduce the scatter on the output (air mass flow rate, predictions indicated with the red dots) as a function of the different input quantities, compared to the original data (black triangles)

indicative metric regarding the scatter, in this paper, the coefficient of variation (COV) is used

$$\mathrm{COV} = \frac{\sigma}{\mu} \tag{3}$$

where σ denotes the standard deviation, calculated using the k-nearest neighbor algorithm, and μ the mean. The metric is calculated for the initial training data and the prediction data for the air mass flow rate (Table 2). The reduction of data-scatter is consistently observed in different noise levels and datasets, due to reductions in the σ and COV indicators, respectively. Consistent results are also derived in the case of amount of water injection (not included in the paper). Finally, the accuracy of the SVR method can be provided by means of an accuracy metric. For the analysis presented in this paper, the coefficient of determination (R^2) is used

$$R^2 = \frac{\sum_i (\hat{y}_i - \bar{y})}{\sum_i (y_i - \bar{y})} \tag{4}$$

where y is the original sample of a dataset, $\hat{y}$ is the corresponding prediction, and $\bar{y}$ the mean of the original dataset. Finally, the calculated metric is 99.1%, which indicates the good prediction capabilities of the underlying SVR model.

To conclude, the clear reduction in COV and standard deviation (σ) indicators (Table 2) highlight thus the potential of the SVR model to reduce the data-scatter. However, currently, this SVR method is only performed on one single datapoint. This analysis still needs to be extended to more operational points and to the actual recuperator performance, before it can be used in an operational monitoring and optimization setting.

5 Conclusion

In this paper, we presented an experimental recuperator performance analysis of an mGT operating under humidified conditions, i.e., as mHAT. The recuperator is responsible for the recovery of extra heat from the flue gases under humidified conditions and its performance has thus a strong influence on the mHAT performance. Finally, this analysis was extended using a SVR model, in a first attempt to obtain this accurate performance.

The experimental analysis allowed to determine the injected water amount, indicating that during most tests, the working fluid was indeed completely saturated. Moreover, the analysis also showed that an additional, considerable amount of liquid water entered the recuperator as well. The analysis of the recuperator performance indicated that, although in water injection operation the global mGT electrical performance increases, the mHAT is not exploiting its full potential. Indeed, the heat flux in the recuperator is, as expected, higher than during dry operation. However, this heat flux is still limited by the limited recuperator size, leading to a lower cold side outlet temperature. Therefore, less heat is recovered than is theoretically possible. Throughout the analysis, a large scatter was observed on all results, highlighting the need for accurate data. In an attempt to improve the accuracy of the real-time data, an SVR model was applied on one specific dataset. This SVR model is capable of reducing the scatter significantly, clearly highlighting its potential for a more accurate online performance determination.

Future work involves the extension of the experimental analysis, by introducing a detailed heat loss model, to obtain an accurate performance map for the recuperator effectiveness as function of flow rate and humidity level. Additionally, the SVR model will be extended toward more and longer datasets. Finally, this model will be used for online monitoring of the recuperator and saturation tower performance. In combination with the performance map, it will enable us to adjust the control settings during operation to receive maximal mGT performance. Once this SVR model is in place, longer and more accurate measurements campaigns can be performed, allowing not only accurate cycle performance, but also more insight on the impact of the humidification on the mGT performance degradation and lifetime on the long term.

Table 2 Reduction in COV and standard deviation (σ) indicators highlight the potential of the SVR model to reduce the data-scatter

Parameter	Training data	Prediction data
μ	0.725790	0.725877
σ	0.001583	0.000893
COV	2.93%	0.71%

Nomenclature

CHP = combined heat and power
CIT = combustor inlet temperature
COV = coefficient of variation
DES = decentralized energy systems
GT = gas turbine
HAT = humid air turbine
mGT = micro gas turbine
mHAT = micro humid air turbine
RE = renewable energy
SM = surge margin
SVR = support vector regression
TIT = turbine inlet temperature
TOT = turbine outlet temperature
VUB = Vrije Universiteit Brussel

References

[1] UNFCCC, 2015, "Paris Agreement," United Nations Climate Change Conference, Bonn, Germany, accessed Dec. 3, 2019, https://unfccc.int/sites/default/files/english_paris_agreement.pdf
[2] Bilgili, M., Ozbek, A., Sahin, B., and Kahraman, A., 2015, "An Overview of Renewable Electric Power Capacity and Progress in New Technologies in the World," Renewable Sustainable Energy Rev., **49**, pp. 323–334.
[3] Elia, 2019, "Elia Releases Its Figures on Belgium's 2018 Energy Mix," Elia, Brussels, Belgium, accessed Dec. 3, 2019, https://www.elia.be/en/news/press-releases/2019/01/20190118_press-release-elia-releases-its-figures-on-belgiums-2018-energy-mix
[4] Montero Carrero, M., De Paepe, W., Parente, A., and Contino, F., 2016, "T100 mGT Converted Into mHAT for Domestic Applications: Economic Analysis Based on Hourly Demand," Appl. Energy, **164**, pp. 1019–1027.
[5] Turbec AB, 2000–2001, "*T100 Microturbine CHP System: Technical Description Ver 4.0*," Turbec AB, Malmö, Sweden.
[6] Jonsson, M., and Yan, J., 2005, "Humidified Gas Turbines—A Review of Proposed and Implemented Cycles," Energy, **30**(7), pp. 1013–1078.
[7] Rao, A. D., 1991, "European Patent Specification," Publication No. 0150990B1.
[8] Bram, S., and De Ruyck, J., 1997, "Exergy Analysis Tools for ASPEN Applied to Evaporative Cycle Design," Energy Convers. Manage., **38**(15–17), pp. 1613–1624.
[9] Parente, J., Traverso, A., and Massardo, A. F., 2003, "Micro Humid Air Cycle—Part A: Thermodynamic and Technical Aspects," ASME Paper No. GT2003-38326.
[10] De Paepe, W., Montero Carrero, M., Bram, S., Contino, F., and Parente, A., 2017, "Waste Heat Recovery Optimization in Micro Gas Turbine Applications Using Advanced Humidified Gas Turbine Cycle Concepts," Appl. Energy, **207**, pp. 218–229.
[11] De Paepe, W., Contino, F., Delattin, F., Bram, S., and De Ruyck, J., 2014, "Optimal Waste Heat Recovery in Micro Gas Turbine Cycles Through Liquid Water Injection," Appl. Therm. Eng., **70**(1), pp. 846–856.
[12] De Paepe, W., Montero Carrero, M., Bram, S., Parente, A., and Contino, F., 2018, "Towards Higher Micro Gas Turbine Efficiency and Flexibility—Humidified mGTs: A Review," ASME J. Eng. Gas Turbines Power, **140**(8), p. 081702.
[13] Zhang, S., and Xiao, Y., 2006, "Steady-State Off-Design Thermodynamic Performance Analysis of a Humid Air Turbine Based on a Micro Turbine," ASME Paper No. GT2006-90335.
[14] Nikpey, H., Mansouri Majoumerd, M., Assadi, M., and Breuhaus, P., 2014, "Thermodynamic Analysis of Innovative Micro Gas Turbine Cycles," ASME Paper No. GT2014-26917.
[15] Majoumerd, M. M., Somehsaraei, H. N., Assadi, M., and Breuhaus, P., 2014, "Micro Gas Turbine Configurations With Carbon Capture—Performance

Assessment Using a Validated Thermodynamic Model," Appl. Therm. Eng., **73**(1), pp. 172–184.
[16] Montero Carrero, M., Ferrari, M. L., De Paepe, W., Parente, A., Bram, S., and Contino, F., 2015, "Transient Simulations of a T100 Micro Gas Turbine Converted Into a Micro Humid Air Turbine," ASME Paper No. GT2015-43277.
[17] Dodo, S., Nakano, S., Inoue, T., Ichinose, M., Yagi, M., Tsubouchi, K., Yamaguchi, K., and Hayasaka, Y., 2004, "Development of an Advanced Microturbine System Using Humid Air Turbine Cycle," ASME Paper No. GT2004-54337.
[18] Nakano, S., Kishibe, T., Araki, H., Yagi, M., Tsubouchi, K., Ichinose, M., Hayasaka, Y., Sasaki, M., Inoue, T., Yamaguchi, K., and Shiraiwa, H., 2007, "Development of a 150 kW Microturbine System Which Applies the Humid Air Turbine Cycle," ASME Paper No. GT2007-28192.
[19] Wei, C., and Zang, S., 2013, "Experimental Investigation on the Off-Design Performance of a Small-Sized Humid Air Turbine Cycle," Appl. Therm. Eng., **51**(1–2), pp. 166–176.
[20] De Paepe, W., Montero Carrero, M., Bram, S., and Contino, F., 2014, "T100 Micro Gas Turbine Converted to Full Humid Air Operation: Test Rig Evaluation," ASME Paper No. GT2014-26123.
[21] De Paepe, W., Montero Carrero, M., Bram, S., and Contino, F., 2015, "T100 Micro Gas Turbine Converted to Full Humid Air Operation: A Thermodynamic Performance Analysis," ASME Paper No. GT2015-43267.
[22] De Paepe, W., Montero Carrero, M., Bram, S., Parente, A., and Contino, F., 2014, "Experimental Characterization of a T100 Micro Gas Turbine Converted to Full Humid Air Operation," Energy Procedia, **61**, pp. 2083–2088.
[23] Montero Carrero, M., De Paepe, W., Magnusson, J., Parente, A., Bram, S., and Contino, F., 2016, "Experimental Characterisation of a Humidified T100 Micro Gas Turbine," ASME Paper No. GT2016-57649.
[24] Montero Carrero, M., De Paepe, W., Magnusson, J., Parente, A., Bram, S., and Contino, F., 2017, "Experimental Characterisation of a Micro Humid Air Turbine: Assessment of the Thermodynamic Performance," Appl. Therm. Eng., **118**, pp. 796–806.
[25] De Paepe, W., Contino, F., Delattin, F., Bram, S., and De Ruyck, J., 2014, "New Concept of Spray Saturation Tower for Micro Humid Air Turbine Applications," Appl. Energy, **130**, pp. 723–737.
[26] Xu, Z., Lu, Y., Wang, B., Zhao, L., Chen, C., and Xiao, Y., 2019, "Experimental Evaluation of 100 kW Grade Micro Humid Air Turbine Cycles Converted From a Microturbine," Energy, **175**, pp. 687–693.
[27] Montero Carrero, M., De Paepe, W., Bram, S., Musin, F., Parente, A., and Contino, F., 2016, "Humidified Micro Gas Turbines for Domestic Users: An Economic and Primary Energy Savings Analysis," Energy, **117**(2), pp. 429–438.
[28] McDonald, C. F., and Rodgers, C., 2005, "Ceramic Recuperator and Turbine: The Key to Achieving a 40 Percent Efficient Microturbine," ASME Paper No. GT2005-68644.
[29] Montero Carrero, M., De Paepe, W., Bram, S., Parente, A., and Contino, F., 2017, "Does Humidification Improve the Micro Gas Turbine Cycle? Thermodynamic Assessment Based on Sankey and Grassmann Diagrams," Appl. Energy, **204**, pp. 1163–1171.
[30] Mahmood, M., Martini, A., Massardo, A. F., and De Paepe, W., "Model Based Diagnostics of AE-T100 Micro Humid Air Turbine Cycle," ASME Paper No. GT2018-75979.
[31] Pedemonte, A., Traverso, A., and Massardo, A., 2008, "Experimental Analysis of Pressurised Humidification Tower for Humid Air Gas Turbine Cycles. Part A: Experimental Campaign," Appl. Therm. Eng., **28**(14–15), pp. 1711–1725.
[32] Parente, J. O., Traverso, A., and Massardo, A. F., 2003, "Saturator Analysis for an Evaporative Gas Turbine Cycle," Appl. Therm. Eng., **23**(10), pp. 1275–1293.
[33] De Paepe, W., Delattin, F., Bram, S., Contino, F., and De Ruyck, J., 2013, "A Study on the Performance of Steam Injection in a Typical Micro Gas Turbine," ASME Paper No. GT2013-94569.
[34] Lee, J. J., Jeon, M. S., and Kim, T. S., 2010, "The Influence of Water and Steam Injection on the Performance of a Recuperated Cycle Microturbine for Combined Heat and Power Application," Appl. Energy, **87**(4), pp. 1307–1316.
[35] De Paepe, W., Renzi, M., Montero Carrerro, M., Caligiuri, C., and Contino, F., 2019, "Micro Gas Turbine Cycle Humidification for Increased Flexibility: Numerical and Experimental Validation of Different Steam Injection Models," ASME J. Eng. Gas Turbines Power, **141**(2), p. 021009.
[36] Lagerström, G., and Xie, M., 2002, "High Performance and Cost Effective Recuperator for Micro-Gas Turbines," ASME Paper No. GT2002-30402.
[37] Renzi, M., Caresana, F., Pelagalli, L., and Comodi, G., 2014, "Enhancing Micro Gas Turbine Performance Through Fogging Technique: Experimental Analysis," Appl. Energy, **135**, pp. 165–173.
[38] Zanger, J., Widenhorn, A., and Aigner, M., 2011, "Experimental Investigations of Pressure Losses on the Performance of a Micro Gas Turbine System," ASME J. Eng. Gas Turbines Power, **133**(8), p. 082302.
[39] De Paepe, W., Delattin, F., Bram, S., and De Ruyck, J., 2013, "Water Injection in a Micro Gas Turbine—Assessment of the Performance Using a Black Box Method," Appl. Energy, **112**, pp. 1291–1302.
[40] De Paepe, W., Montero Carrero, M., Giorgetti, S., Parente, A., Bram, S., and Contino, F., 2016, "Exhaust Gas Recirculation on Humidified Flexible Micro Gas Turbines for Carbon Capture Applications," ASME Paper No. GT2016-57265.
[41] Bellman, R., 1961, *Adaptive Control Processes: A Guided Tour*, Princeton University Press, Oxford, London, UK.
[42] Smola, A., and Schölkopf, B., 2004, "A Tutorial on Support Vector Regression," Stat. Comput., **14**(3), pp. 199–222.
[43] Chen, K.-Y., 2007, "Forecasting System Reliability Based on Support Vector Regression With Genetic Algorithms," Reliab. Eng. Syst. Saf., **92**(4), pp. 423–432.
[44] Cherkassky, V., and Ma, Y., 2004, "Practical Selection of Svm Parameters and Noise Estimation for SVR Regression," Neural Networks, **17**(1), pp. 113–126.
[45] Ito, K., and Nakano, R., 2003, "Optimizing Support Vector Regression Hyperparameters Based on Cross-Validation," Proceedings of the International Joint Conference on Neural Networks, Portland, OR, July 20–24, pp. 2077–2082.
[46] Che, J., 2013, "Support Vector Regression Based on Optimal Training Subset and Adaptive Particle Swarm Optimization Algorithm," Appl. Soft Comput., **13**(8), pp. 3473–3481.
[47] Megri, F., Megri, A., and Djabri, R., 2016, "An Integrated Fuzzy Support Vector Regression and the Particle Swarm Optimization Algorithm to Predict Indoor Thermal Comfort," Indoor Built Environ., **25**(8), pp. 1248–1258.
[48] Michalewicz, Z., 1995, "Genetic Algorithms Numerical Optimization and Constraints," Proceedings of the Sixth International Conference on Genetic Algorithms, Pittsburgh, PA, July 15–19, pp. 151–158.
[49] Tsirikoglou, P., Abraham, S., Contino, F., Lacor, C., and Ghorbaniasl, G., 2017, "A Hyperparameters Selection Technique for Support Vector Regression Models," Appl. Soft Comput., **61**, pp. 139–148.